# LARGE EDDY SIMULATION OF TURBULENT DUCT FLOWS IN A LIQUID METAL MHD GENERATOR WITH NON-UNIFORM MAGNETIC FIELD

**Hiromichi Kobayashi**
Department of Physics
Keio University
4-1-1, Hiyoshi, Kohoku-ku, Yokohama 223-8521, Japan
hkobayas@phys-h.keio.ac.jp

**Hiroki Shionoya, Yoshihiro Okuno**
Department of Energy Sciences
Tokyo Institute of Technology
4259 Nagatsuta-cho, Midori-ku, Yokohama 226-8503, Japan
shionoya.h.aa@m.titech.ac.jp, yokuno@es.titech.ac.jp

## ABSTRACT

Large-eddy simulation (LES) of the turbulent duct flows in a liquid metal magnethydrodynamic (MHD) power generator is examined to reveal the behavior of the MHD flows and the turbulent structures. The non-uniform magnetic flux density in the streamwise direction produces two eddy currents. The eddy current causes the wall-jet flows with M-shaped mean streamwise velocity profiles in the direction parallel to the external magnetic field. In contrast, the Hartmann flows with the flattened velocity profiles by the Lorentz force are produced in the direction perpendicular to the external magnetic field. In the case of the strong magnetic flux density, the turbulence structures similar to the Karman vortex sheets emerge in the downstream duct. The coherent structure model, one of the subgrid-scale models, well represents the relaminarization by the Lorentz force in comparison with the Smagorinsky model with the Van Driest's wall function. Turbulence intensities decrease under the magnetic field, but in the wall jet flows, the streamwise one is enhanced.

## INTRODUCTION

A magnetohydrodynamic (MHD) electrical power generator directly converts the enthalpy of a flow to electrical energy without rotating parts (Rosa, 1968). When a magnetic field is applied to a liquid metal flow, the electric current is generated and the electric power is extracted via an external load resistance connected between opposed electrodes. Since the liquid metal possesses extremely high electrical conductivity compared to plasma, the energy conversion can be effectively achieved even for low speed liquid metal flows.

The experiments of the liquid metal MHD generators have been carried out (Maeda, 2003; Elliot, 1966; Satake et al., 2008), whereas the LES (Shimomura, 1991; Kobayashi, 2006; Sarris, 2007) and DNS (Satake, 2006; Boeck, 2007) of the MHD channel flows in the uniform magnetic field have been conducted as well as the MHD duct flows (Kobayashi, 2008).

In a practical generator, the external magnetic field is applied in between a finite width which depends on a magnet size. It is of great importance to clarify the influence of finite, non-uniform magnetic field on turbulent flows as well as generator performance. The M-shaped velocity profiles, the so-called wall-jet flow, were confirmed in experiments (Reed and Lykoudis, 1978; Andreev et al., 2006) and numerical simulations (Yamada et al., 2004; Yamada et al., 2005; Kakizaki et al., 2003).

In this study, LES with the coherent structure model (CSM) (Kobayashi, 2005) applicable to the MHD turbulent flows is conducted to reveal turbulent phenomena in a liquid metal MHD generator with a square duct to which non-uniform magnetic field is applied.

## GOVERNING EQUATIONS AND NUMERICAL CONDITIONS

The governing equations of liquid metal flows consist of a continuity equation and Navier-Stokes equations with the Lorentz force for incompressible flows. In addition, Maxwell equations are solved simultaneously. In this study, there is a possibility that the magnetic Reynolds number reaches unity, so that we consider the induced magnetic fields $\vec{B}_i$. An external magnetic field is applied to the generator only in the $z$ direction, that is, $\vec{B}_0$=(0,0,$Bz_0$). Thus, total magnetic fields are set to $\vec{B} = \vec{B}_0 + \vec{B}_i$. The governing equations are listed below.

(i) Continuity equation:

$$\nabla \cdot \vec{u} = 0 \tag{1}$$

(ii) Navier-Stokes equations:

$$\frac{\partial \vec{u}}{\partial t} + \nabla \cdot (\vec{u}\vec{u}) = -\frac{1}{\rho}\nabla P + \frac{\partial \tau_{ij}}{\partial x_j} + \frac{1}{\rho}\vec{j} \times \vec{B} \tag{2}$$

(iii) Maxwell equations:

$$\nabla \times \vec{E} = \frac{\partial \vec{B_i}}{\partial t}\ ,\quad \nabla \times \vec{B_i} = \mu_0 \vec{j} \tag{3}$$

(iv) Ohm's law:

$$\vec{j} = \sigma\left(\vec{E} + \vec{u} \times \vec{B}\right) \tag{4}$$

Here, we use the so-called *A*-$\phi$ method for the vector potential $\vec{A}$ and the electric potential $\phi$ to obtain the electric field $\vec{E}$ and the induced magnetic field $\vec{B}_i$, and we adopt the Coulomb gage $\nabla \cdot A = 0$. Then, we have the following equations.

(v) Poisson equation for the electric potential:

$$\nabla^2 \phi = \nabla \cdot \left(\vec{u} \times \vec{B}\right) \tag{5}$$

(vi) Poisson equations for the vector potentials:

$$\nabla^2 \vec{A} = -\mu_0 \vec{j} \tag{6}$$

where

$$\vec{E} = -\nabla\phi - \frac{\partial \vec{A}}{\partial t}\ ,\qquad \nabla \times \vec{A} = \vec{B_i} \tag{7}$$

The central finite difference method with the second order accuracy is used. The time-marching scheme is the Adams-Bashforth method with the second order accuracy. The SMAC method is adopted for the coupling scheme between velocity and pressure. The Poisson equations are solved with Bi-CGSTAB method.

The subgrid-scale stress tensor $\tau_{ij}$ is modeled by the coherent structure model (CSM) (Kobayashi, 2005) based on the turbulence structure. This model gave good results not only for the flows around the complex geometries but also for the MHD turbulent flows The model parameter *C* is determined locally without averaging and clipping. The model is expressed as follows.

$$\tau_{ij} = -2C\Delta^2 |S| S_{ij} \tag{8}$$

$$C = \frac{1}{22}|Fcs|^{3/2}(1 - Fcs) \tag{9}$$

$$Fcs = Q/E \tag{10}$$

$$Q = \frac{1}{2}\left(W_{ij}W_{ij} - S_{ij}S_{ij}\right) \tag{11}$$

$$E = \frac{1}{2}\left(W_{ij}W_{ij} + S_{ij}S_{ij}\right) \tag{12}$$

$$S_{ij} = \frac{1}{2}\left(\frac{\partial u_j}{\partial x_i} + \frac{\partial u_i}{\partial x_j}\right) \tag{13}$$

$$W_{ij} = \frac{1}{2}\left(\frac{\partial u_j}{\partial x_i} - \frac{\partial u_i}{\partial x_j}\right) \tag{14}$$

where *Q* is the second invariant of the velocity gradient tensor and *E* is the magnitude of the velocity gradient tensor. The iso-surface of *Q* is often used to visualize eddies. This model assumes that the energy transfer from the grid scale to the subgrid scale takes place around the eddies. *Fcs* is the coherent structure function, and its absolute value is less than unity.

The schematic view of the computational domain is shown in Fig. 1. The magnetic flux density imposed externally is shown in Fig. 2. The external magnetic field is induced toward the + *z* direction, and it has no distribution in the *y* and *z* directions. The liquid metal flows toward the + *x* direction. The staggered grid is used for velocity. The equally spaced gird is used in the *x* direction ($\Delta x = 1.57\times10^{-2}$mm, $\Delta x^+ = 70.7$)), and the stretched grid is adopted in the *y* and *z* directions ($\Delta y$, $\Delta z = 2.48\times10^{-4}$~$2.41\times10^{-3}$mm, $\Delta y^+$, $\Delta z^+ = 1.12$~10.8). The grid size is 36, 64, and 64 for *x*, *y*, and *z*, respectively. The time step is $\Delta t = 1\times10^{-2}$m/s. The U-Alloy ($\sigma = 2.31\times106$S/m, $\nu_m = 3.11\times10^{-7}$m$^2$/s) is assumed as the liquid metal, and the electrode is made of cupper ($\sigma = 5.90\times10^7$S/m). We call the generation region located in between electrodes and $x = 0.27$~0.33m. The central position in the *y* and *z* directions are $y = 0.04$m and $z = 0.04$m, respectively. The electrode has the lengths 0.063m, $4.87\times10^{-3}$m, 0.08m in *x*, *y*, and *z* directions, respectively. The electric wire is connected at the center of the outer surface of the electrode in the *x*-*z* plane. The maximum magnetic flux density is 0.12T, and the external load resistance is set to $2.0\times10^{-6}$ Ω.

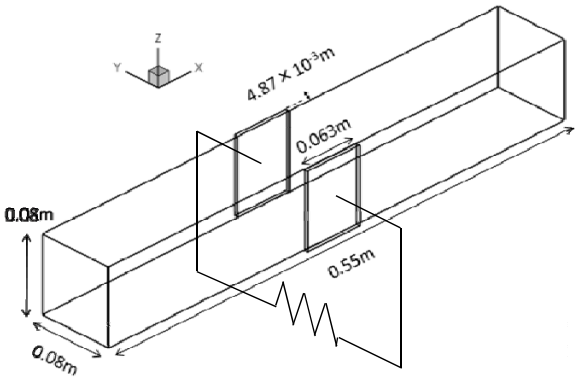

Figure 1 Schematic of MHD power generator.

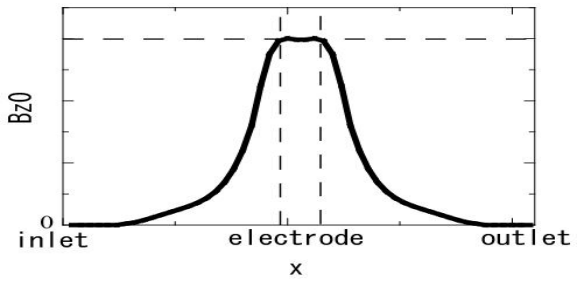

Figure 2 The profile of the external magnetic field.

For the inlet condition, the fully developed turbulent duct flow at $Re\tau = 180$ is given sequentially. The convective outflow condition is used for the outlet condition. The non-slip condition is imposed on the walls. The non-penetration condition is given for the insulated walls, and the penetration condition is imposed for the electrodes.

## NUMERICAL RESULTS

Figure 3 shows the instantaneous velocity distributions in the *x*-*y* and *x*-*z* planes at 0.12T. When the external magnetic flux density of 0.12T is applied, the difference between the *x*-*y*

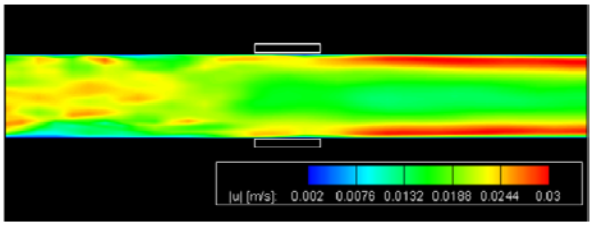


(a) Central *x*-*y* plane

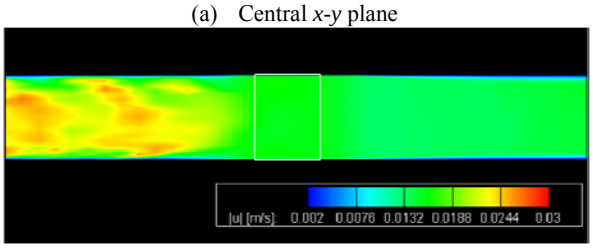


(b) Central *x*-*z* plane

Figure 3 Instantaneous velocity distributions at 0.12T.

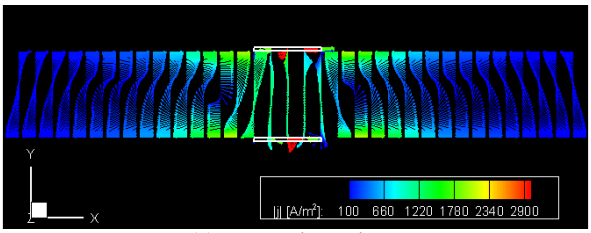


(a) Central *x*-*y* plane

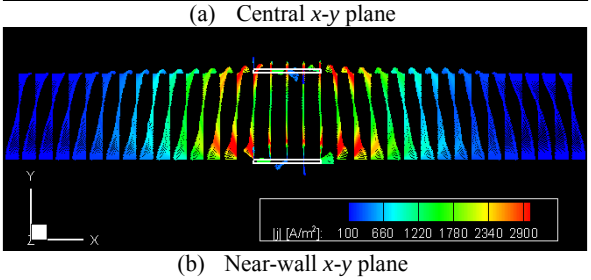


(b) Near-wall *x*-*y* plane

Figure 4 Vector distributions of electric current density.

and *x*-*z* planes appears obviously. In the generation region between electrodes, the Lorentz force acts against the flow, and the turbulent flow is uniformly suppressed. In the downstream region of the *x*-*y* plane, the wall-jet flows emerge, whereas in the *x*-*z* plane the velocity distribution becomes uniform. The wall-jet flows never appear when the external magnetic field is uniformly imposed. The wall-jet flow is induced by the non-uniform, external magnetic field.

Fig. 4 shows the vector distributions of the electric current density in the central and the near-wall *x*-*y* plane. Note that the color shows the magnitude of the electric current density, but the same vector length is used for the purpose of easy view. In the central plane, the electric current flows from the anode to the cathode, namely, toward the –*y* direction. On the other hand, in the near-wall plane, the electric current inversely flows. This inverse flow is due to the low velocity near the wall in Eq. (4).

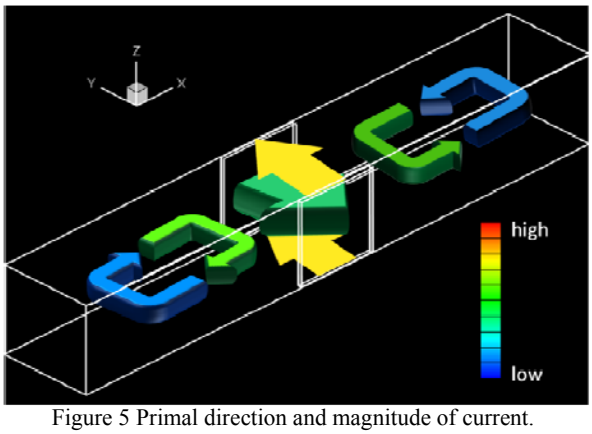


Figure 5 Primal direction and magnitude of current.

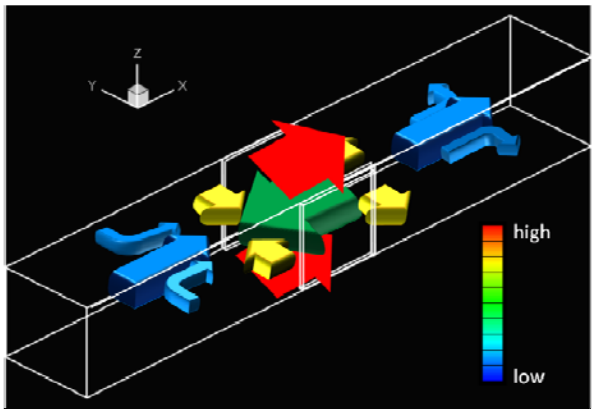


Figure 6 Primal direction and magnitude of Lorentz force.

Figures 5 and 6 show the schematic view of the direction and the magnitude of the primal electric current and Lorentz force. We can see two eddy currents in the upstream and downstream regions, and the eddy currents give the different orientation to the Lorentz force in the *y* direction.

We compared the viscosity between CSM and Smagorinsky model with the van Driest's wall function in Fig. 7. In the wall jet region, the Smagorinsky model gives high turbulent viscosity in connection with the strong mean velocity gradient, whereas the CSM predicts relaminarization properly.

Let us compare the mean streamwise velocity profiles in the central *x*-*y* and *x*-*z* planes for various *x* positions indicated in Fig. 8. Figure 9 shows the mean streamwise velocity profiles for 0T and 0.12T. The mean velocity profiles in the central *x*-*y* and *x*-*z* planes are no difference at 0T. In contrast, at 0.12T the so-called M-shaped profiles are shown in the central *x*-*y* plane. Those are the wall-jet flows. In the central *x*-*z* plane, velocity profiles at the center of duct are flattened in the downstream region. However, the near-wall velocity profiles in the generation region deviate from the conventional one. The boundary layer is called the Hartman layer with an exponential distribution.

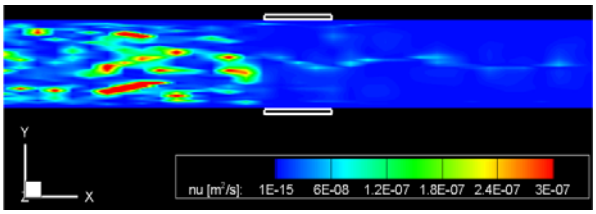


(a) coherent structure model

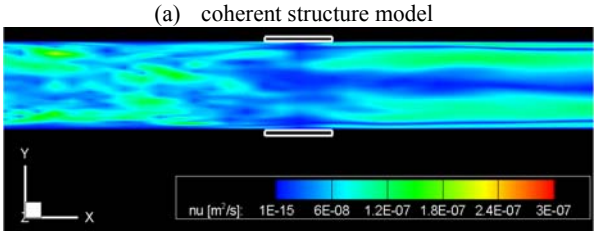


(b) Smagorinsky model

Figure 7 Viscosity distributions in the central *x*-*y* plane.

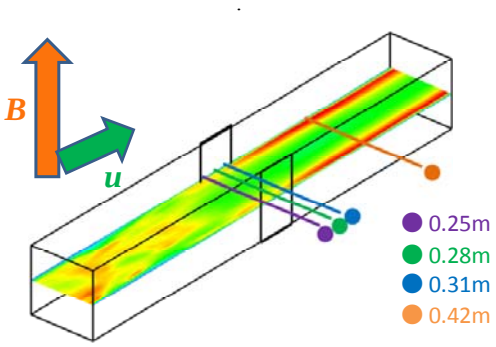


(a) central *x*-*y* plane

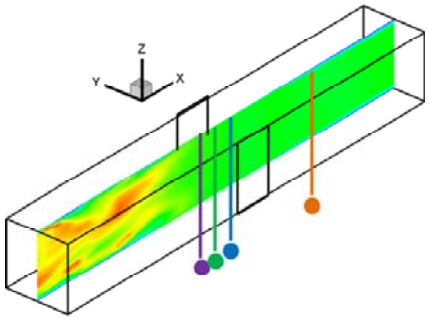


(b) central *x*-*z* plane

Figure 8 Mesurement points in the central *x*-*y* and *x*-*z* planes.

Figures 10 and 11 show the Reynolds stress profiles and streamwise turbulence intensities. The Reynolds stress is suppressed to be nearly zero at the all measured points. The streamwise turbulence intensities are also suppressed gradually from inlet to outlet. In the wall-jet region, we can see the enhancement of turbulence intensity (orange line).

Figure 12 shows the turbulence structures for 0.12T and 0.06T. The iso-surface of the second invariant $Q$=0.02 is visualized in the left figures and in addition the iso-surface of

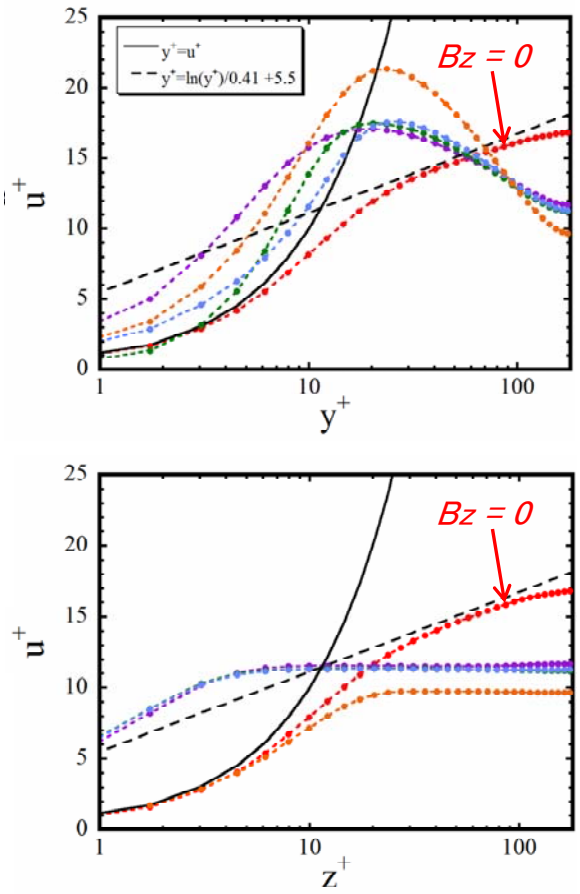


Figure 9 Mean streamwise velocity profiles at 0T and 0.12T.

$u^+v^+=\pm 5.0$ is shown in the right figures. For 0.12T, the eddy structures are suppressed in the generation region, and from the downstream end of the electrode Karman vortex sheets emerge and the turbulence structure align in the direction where the external magnetic field is applied. For 0.06T, the suppression of eddies becomes weak.

## SUMMARY

In order to clarify the turbulence phenomena in the liquid metal MHD power generator, LES was carried out, and the behavior of the MHD flows and the turbulence structures were examined. The following summary was drawn.

The non-uniform magnetic flux density in the streamwise direction produces the eddy currents in the upstream and downstream regions. The eddy current causes the Hartmann flow with the flattened velocity profiles in the direction perpendicular to the external magnetic field and the M-shaped velocity profiles in the direction parallel to the external magnetic field. The Reynolds stress is reduced to be zero, and streamwise turbulence intensities are decrease from inlet to outlet. In the wall-jet region, it is found that the streamwise

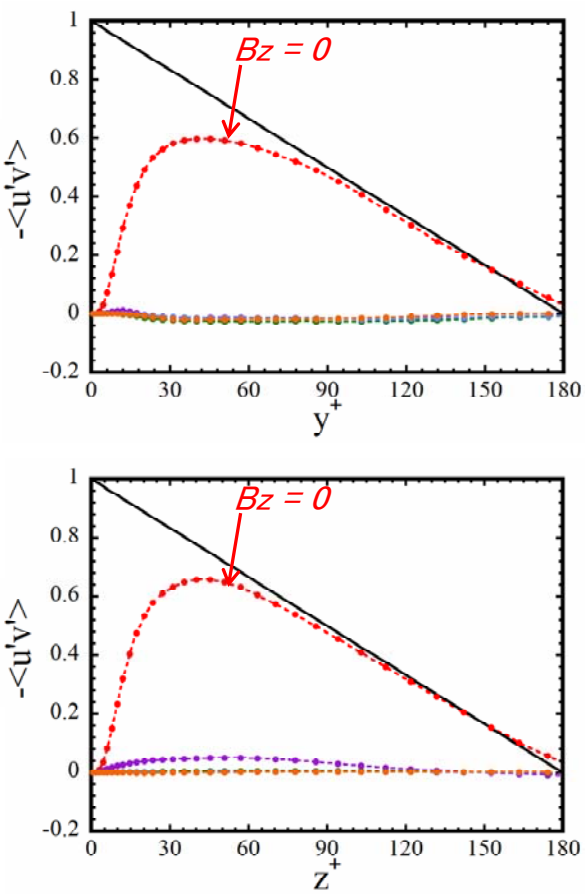


Figure 10 Reynolds stress profiles at 0T and 0.12T.

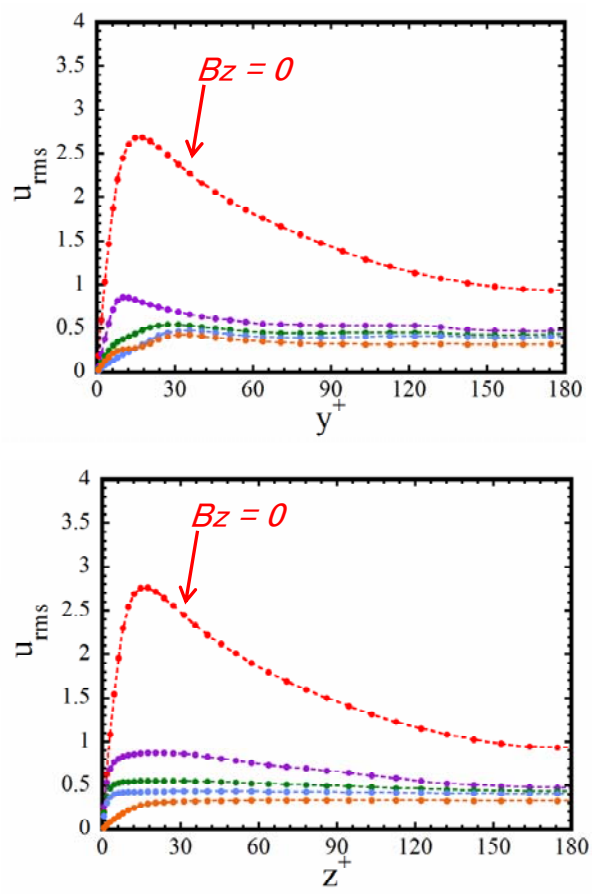


Figure 11 Streamwise turbulence intensites at 0T and 0.12T.

turbulence intensity is enhanced. Turbulence suppression increases in the magnetic flux density. The strong magnetic field, however, develops the turbulence structure similar to the Karman vortex sheets for Reynolds stress. Furthermore, it is confirmed that the coherent structure model of the subgrid scale model represents the relaminarization better than the Smagorinsky model.

## REFERENCES


Andreev, O., Kolesnikov, Yu., and Thess, A., 2006, "Experimental study of liquid metal channel flow under the influence of a nonuniform magnetic field", *Phys. Fluids*, Vol.18, 065108.

Boeck, T., Krasnov, D., and Zienicke, E., 2007, "Numerical study of turbulent magnetohydrodynamic channel flow", *J. Fluid Mech.*, Vol.572, 179-188

Elliott D. G., 1966, "Direct Current Liquid-Metal Magnetohydrodynamic Power Generator", *AIAA Journal*, Vol.4, No.4, pp.627-634.

Kakizaki, K., Maeda, T., Ishikawa, M., 2003, "MHD simulation of liquid Metal MHD power generator: Effect of Magnetic field distribution on the generator performance", *Proceedings of Thermal Engineering Conference*, Vol.2003, pp. 379-380.

Kobayashi, H., 2005, "The subgrid-scale models based on coherent structures for rotating homogeneous turbulence and turbulent channel flow", *Phys. Fluids* 17, 045104.

Kobayashi, H., 2006, "Large eddy simulation of magnetohydrodynamic turbulent channel flows with local subgrid-scale model based on coherent structure", *Phys. Fluids*, Vol.18, 045107.

Kobayashi, H., 2008, "Large eddy simulation of magnetohydrodynamic turbulent duct flows", *Phys. Fluids*, Vol.20, 015102.

Maeda, T., 2003, "The fundamental characteristics of liquid metal MHD engine generator", *Journal of the Japan Society of Applied Electromagnetics*, Vol.11, No.4, pp.249-255.

Reed, C. B., Lykoudis, P. S., 1978, "The effect of a transverse magnetic field on shear turbulence", *J. Fluid Mech.*, Vol.89, pp.147-171.

Rosa, R. J., 1968, *Magnetohydrodynamic Energy Conversion*, McGraw-Hill, New York.

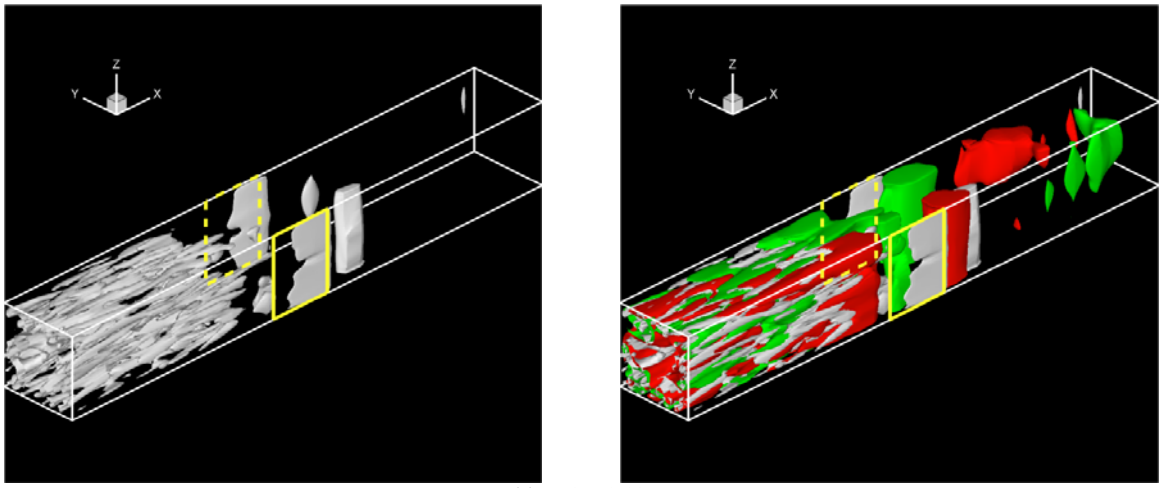


(a) Bz0 = 0.12T

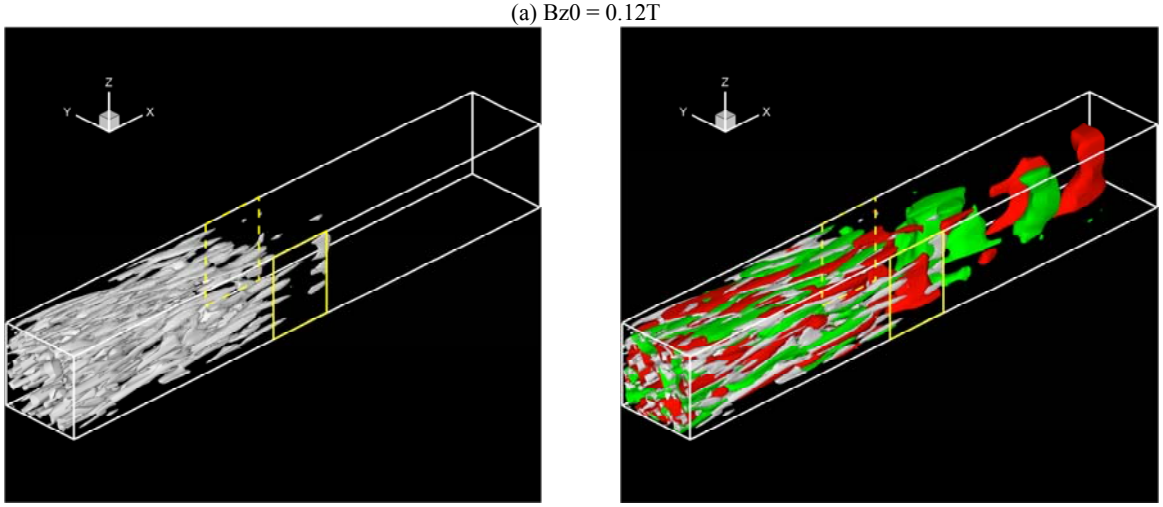


(b) Bz0 = 0.06T

Figure 12 Turbulence structures at (a) 0.12T and (b) 0.06T; left: second invariant Q=0.02; right: $u^+v^+=\pm 5.0$.

Sarris, I. E., Kassinos, S. C., Carati, D., 2007, "Large-eddy simulations of the turbulent Hartmann flow close to the transitional regime". *Phys. Fluids*, Vol.19, 085109.

Satake, S., Fujino, T., Ishikawa, M., Maeda, T., 2008, "Experimental Study of Proof-of-Principle of Liquid Metal MHD Generation", *New energy technology symposium*, B-1-4.

Satake, S., Kunugi, T., Takase, K.., Ose, Y., 2006, "Direct numerical simulation of turbulent channel flow under a uniform magnetic field for large-scale structures at high Reynolds number", *Phys. Fluids*, Vol.18, 125106.

Shimomura, Y., 1991, "Large eddy simulation of magnetohydrodynamic turbulent channel flows under a uniform magnetic field", *Phys. Fluids*, Vol.A 3 pp.3098.

Yamada, K., Maeda, T., Hasegawa, Y., Okuno, Y., 2004, "Two-dimensional Numerical Simulation on Performance of Liquid Metal MHD Generator", *The transactions of the Institute of Electrical Engineers of Japan.*, B, A publication of Power and Energy Society, 124(7), pp.971-976.

Yamada, K., Maeda, T., Hasegawa, Y., Okuno, Y., 2005, "Three-dimensional Numerical Simulation on Performance of Liquid Metal MHD Generator", *The transactions of the Institute of Electrical Engineers of Japan.*, B, A publication of Power and Energy Society, 125(2), pp.141-146.